



Terpene speciation: Analytical insights into the oxidation and pyrolysis of limonene and 1,8-cineole via molecular-beam mass spectrometry

Thomas Bierkandt^{*}, Nina Gaiser, Jasmin Bachmann, Patrick Oßwald, Markus Köhler

Institute of Combustion Technology, German Aerospace Center (DLR), Stuttgart, Germany

ARTICLE INFO

Keywords:

Terpenes
Limonene
1,8-Cineole
Molecular-beam mass spectrometry (MBMS)
Oxidation and pyrolysis

ABSTRACT

Comprehensive speciation datasets for the stoichiometric oxidation and pyrolysis of the two monoterpenes limonene ($C_{10}H_{16}$) and 1,8-cineole ($C_{10}H_{18}O$) are measured in an atmospheric laminar flow reactor using electron-ionization molecular-beam mass spectrometry. This setup allows direct sampling from the reactive flow and preserves the actual gas composition. Furthermore, clear determination of the exact elemental composition of the formed species is possible with the used time-of-flight mass spectrometer. Limonene is a monocyclic terpene and 1,8-cineole is a saturated bicyclic terpene ether and both terpenes might be potential biofuel candidates. Focus in this study is the intermediate temperature region between 673 and 1173 K to obtain insights into the first fuel decomposition steps and the formation of typical soot precursors. The obtained mole fraction profiles for over 40 species in each of the investigated terpenes are a first step for future development and validation of chemical kinetic combustion mechanisms. While the overall species pool is similar, significant concentration differences can be observed for certain combustion intermediates. For limonene, larger quantities of C_8 – C_{10} hydrocarbons are detected and most of them are probably substituted benzenes or cyclohexadienes formed from hydrogen abstraction. Some reaction steps in the decomposition of limonene may also involve initial isomerization of the fuel molecule. In contrast, direct formation of C_7H_{11} radicals and acetone (C_3H_6O) is identified as an important decomposition step of 1,8-cineole. C_7H_{11} is then a source of toluene (C_7H_8) and cyclohexadienes (C_6H_8). Generally, a higher sooting propensity of limonene compared to 1,8-cineole can be expected due to the higher concentrations of polycyclic aromatic hydrocarbons (PAHs) in the investigated temperature range. During limonene oxidation, formation of oxygenated species larger than the fuel molecule are observed and might represent carbonyls or cyclic ethers from the first oxygen addition due to low-temperature chemistry.

1. Introduction

Limonene ($C_{10}H_{16}$) and 1,8-cineole ($C_{10}H_{18}O$) are naturally occurring monoterpenes in orange and eucalyptus oil, and are widely used as fragrances. Both of these essential oils may also be suitable as renewable blending components with conventional diesel fuel and were already tested with diesel up to 10 % by volume [1]. Both essential oils-diesel blends emitted less CO and NO_x but more particulate matter (PM) compared to neat diesel [1]. Table 1 shows the chemical structures of both terpenes together with some engine-relevant properties, e.g., research octane number (RON) or derived cetane number (DCN).

1,8-Cineole, also known as eucalyptol, is a saturated bicyclic ether with comparable motor octane number to ethanol but significantly higher energy density and could potentially also be suitable for spark-

ignition (SI) engines [4]. Limonene is a monocyclic terpene, also discussed as an octane booster in low-octane hydrocarbons due to change in molecular interaction energy [5] and tested as additive to *n*-heptane and low-octane gasoline in a spark-ignition engine [6]. Hydrogenation of limonene to *p*-menthane ($C_{10}H_{20}$) gives access to a high-energy density jet fuel component [7]. Cycloaddition reactions of limonene and other monoterpenes are also in discussion to obtain high-performance jet fuel blendstocks [3,8]. As for many other terpenes, biosynthetic production routes of limonene and 1,8-cineole by engineered bacteria are under investigation [9]. Limonene production is also possible from pyrolysis of waste tires [10,11].



Despite their potential as biofuels, studies on the combustion kinetics of limonene and 1,8-cineole are very limited. Kumar et al. showed that blends of limonene (10, 30, and 50 vol%) have better spray combustion

^{*} Corresponding author at: German Aerospace Center (DLR), Pfaffenwaldring 38-40, 70569 Stuttgart, Germany.

E-mail address: thomas.bierkandt@dlr.de (T. Bierkandt).

Table 1

Chemical structures of the two investigated monoterpenes limonene and 1,8-cineole and some engine-relevant properties.

Terpene	Limonene	1,8-Cineole
Molecular formula	C ₁₀ H ₁₆	C ₁₀ H ₁₈ O
Structural formula		
Molar mass / g/mol	136.23	154.25
Density at 25 °C / g/mL	0.84 [2]	0.93 [2]
Lower heating value / MJ/L	36.1 [3]	36.28 [2]
Research octane number (RON)	87.1 [2]	99.2 [2]
Derived cetane number (DCN)	19.0 [2]	18.8 [2]

characteristics with lower CO emissions compared to neat Jet A-1 [12]. The low-temperature combustion of limonene was studied in a jet-stirred reactor (JSR) between 520 and 800 K by online Fourier transform infrared (FTIR) spectroscopy and high-resolution mass spectrometry and formation of highly-oxidized products from autoxidation, the Korcek mechanism, and the Waddington mechanism was observed [13,14]. Under low-temperature conditions, a broad range of oxygenated species containing four or more oxygen atoms [13], aromatics, and polyunsaturated products [14] are formed during oxidation of limonene. Those oxidation products may have an impact on particulate formation when released into troposphere [13,14]. Autoxidation products for limonene were also experimentally investigated in a jet-stirred reactor at 590 K by liquid chromatography, flow injection, and soft-ionization high-resolution mass spectrometry [15]. Pisarenko et al. developed a kinetic model for the autoxidation of limonene, which includes the initiation reaction of limonene with O₂ to form a limonene radical and HO₂, propagation reactions leading to the formation of limonene peroxides and hydroperoxides, as well as branching and termination reactions [16]. General combustion characteristics (laminar burning speeds, Markstein lengths, and flame thicknesses) were determined by Courty et al. for limonene/air mixtures in a spherical combustion chamber at atmospheric pressure and elevated temperatures [17]. While most the previous work focuses on species identification during low-temperature oxidation of limonene, Pines and Ryer studied the pyrolysis of limonene over copper pellets at 450 °C and atmospheric pressure [18]. They identified aromatic hydrocarbons (*p*-cymene, *m*-xylene, 1,2,3,5-tetramethylbenzene, and trimethylbenzenes) and alkylcyclohexanes as major constituents and proposed formation pathways [18].

For 1,8-cineole, the chlorine-initiated oxidation was studied experimentally [19] and via a combination of experimental and theoretical methods [20,21]. Imwinkelried et al. identified three ketones (acetone, 3,3-trimethyl-2-oxabicyclo[2.2.2]octan-5-one and 1,3,3-trimethyl-2-oxabicyclo[2.2.2]octan-6-one) by gas chromatography-mass spectrometry as products during chlorine-initiated oxidation of 1,8-cineole at 298 K and atmospheric pressure [19]. Gao also computed Arrhenius parameters and rate constants at 600 K for hydrogen abstraction by chlorine and CH₃ radicals from 1,8-cineole and the subsequent reactions of the major alkyl radicals [21]. Corchnoy and Atkinson determined rate constants for the gas-phase reactions of OH and NO₃ radicals with 1,8-cineole [22]. All of this work about 1,8-cineole focuses on low-temperature conditions. General studies on the sooting propensity of limonene and 1,8-cineole were recently performed by Zhu et al. [23] and Yin et al. [24]. Both yield sooting index (YSI) measurements in methane-doped flames [23] and smoke point (SP) determinations using a wick-fed burner [24] showed a higher sooting tendency of limonene compared to 1,8-cineole.

There are hardly any studies on the combustion of limonene and 1,8-cineole under typical high-temperature conditions. We have therefore

Table 2

Inlet flow conditions and investigated temperature ranges for the studied terpene fuels.

Terpene	Limonene		1,8-Cineole	
Equivalence ratio (Φ)	1.0	∞	1.0	∞
Fuel / sccm ¹	5	5	5	5
O ₂ / sccm ¹	70	-	70	-
Ar / slm ²	9.9	9.9	9.9	9.9
Temperature / K	673–1273		773–1273	

¹ sccm: standard cubic centimeters per minute at 1 atm and 273.15 K.

² slm: standard liter per minute at 1 atm and 273.15 K.

investigated the oxidation and pyrolysis of limonene and 1,8-cineole in an atmospheric laminar flow reactor by electron-ionization (EI) molecular-beam mass spectrometry (MBMS) between 673 and 1273 K to gain insights into the fuel decomposition and the formation of important intermediates.

2. Experiment

Stoichiometric oxidation ($\Phi = 1$) and pyrolysis ($\Phi = \infty$) of both terpenes, i.e., limonene ((R)-(+)-limonene, 97 %, Alfa Aesar) and 1,8-cineole (99 %, Alfa Aesar), were studied under comparable conditions with the same carbon flow of 50 sccm, i.e., 5 sccm limonene and 1,8-cineole, respectively. Contained impurities in the used limonene were determined by comprehensive two-dimensional gas chromatography-mass spectrometry (GCxGC-MS), typically used to analyze compositions of real fuels, e.g., gasoline, kerosene, or diesel, see Melder et al. [25].

To prevent any heat release from self-sustainable combustion, a very high dilution with more than 99 % of the inert gas argon with a flow of 9.9 slm is used in the performed flow reactor experiments. For the oxidation measurements, the additional flow rate of molecular oxygen (O₂) as oxidizer was 70 sccm. Table 2 summarizes the applied flow conditions and the investigated temperature ranges.

The liquid fuels were vaporized slightly below their boiling points at 171 °C for limonene and 173 °C for 1,8-cineole in a commercial vaporizer (Bronkhorst® model W-102A CEM) with argon as carrier gas and transferred to the reactor by a heating hose at 150 °C. With 99 % argon dilution, the partial pressure of both fuels is lower than their vapor pressure at atmospheric pressure and room temperature so that condensation is not possible. The liquid fuels and gases (Ar and O₂) are metered by Coriolis mass flow controllers (Bronkhorst® mini CORIFLOW). For the oxidation measurements, the diluted fuel flow was only mixed with oxygen directly at the inlet of the reactor. Note that the oxygen stream was also diluted in argon and preheated prior to being mixed with the fuel stream. Since the inlet of the reactor is more than 300 mm long before the heated isothermal reaction segment of the reactor is reached, properly mixing is achieved under the investigated flow conditions.

The flow reactor consists of a quartz tube with an inner diameter of 40 mm and a length of 1457 mm that is gas-tight mounted in a water-cooled stainless-steel flange at the inlet. The temperature of the inlet flange was regulated to 55 °C by a heating circulator (Lauda model ECO E 4 S). The reactor temperature was varied from 400 to 1000 °C (673–1273 K) by a split tube furnace with a heated length of 1040 mm (Carbolite Gero model FZS 13/40/1000). A sample is withdrawn directly from the hot gas stream at the reactor outlet by a quartz nozzle and transferred through a two-stage expansion into the ionization chamber of the reflectron time-of-flight mass spectrometer (Kaesdorf, $m/\Delta m = 3000$ at m/z 28). Due to the large pressure drop from atmosphere to about 10⁻³–10⁻⁴ mbar, a molecular-beam is formed and the composition at the time of sampling is preserved, i.e., all chemical reactions are quenched. The used EI-MBMS system allows the determination of the exact element composition and species profiles are obtained as function of the oven temperature. A detailed description of

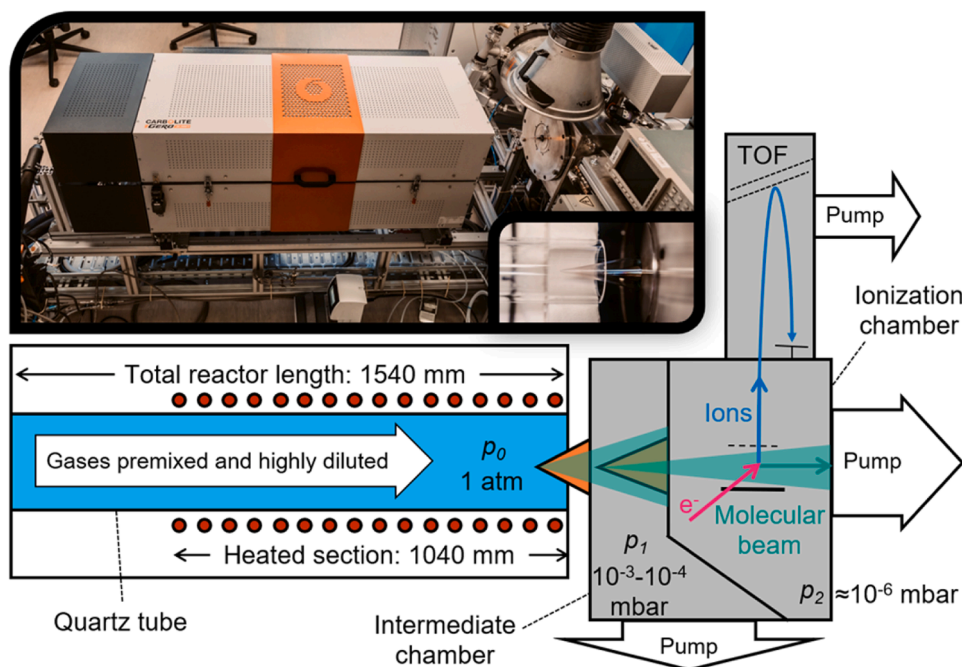


Fig. 1. Schematic and photo of the EI-MBMS system coupled to an atmospheric flow reactor.

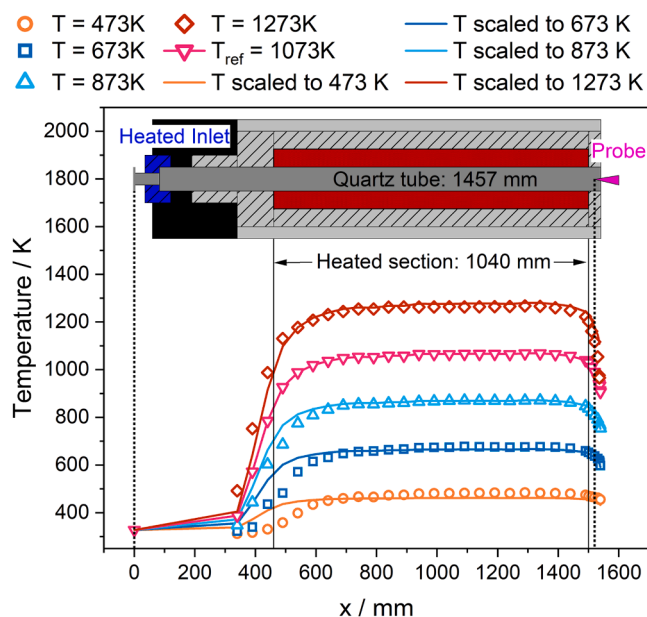


Fig. 2. Measured centerline gas temperature profiles for five oven temperatures and scaled temperature profiles as function of the longitudinal reactor position x .

the used EI-MBMS setup can also be found in [26] and a schematic of the experimental setup is given Fig. 1. The used flow reactor tube has the same dimensions as used before to assume plug flow assumptions for simulations (see [26]). The molecular Péclet number of the reactor is 48–60 and the axial Péclet number is 3.7–3.0 for temperatures between 1273 and 773 K and is also comparable to other laminar flow reactors with plug flow assumption, e.g., Rasmussen et al. [27]. Under the investigated conditions with 99 % argon dilution and a flow rate of 9.9 slm, the Reynolds number is 143–200 for temperatures between 1273 and 773 K and fulfils the criteria of a laminar flow. The reactor diameter is chosen large enough to ensure the dominance of gas phase reactions

and a significant difference of wall and centerline temperatures was not observed in the heated length of the presented reactor in this work (see Fig. S1) and in a previous work of Obwald and Köhler [26] for a similar reactor.

The oven temperature was continuously varied with 200 K/h and the averaging time of the mass spectrometer was chosen such that each data point represents a temperature change of only 2.5 K. Stability of the continuous measurement strategy was tested for a reactive methane mixture in our previous work and reproducibility of the results was found to be excellent [26]. The nominal ionization energy was set to 13.5 eV, which is a good tradeoff between sufficient signal intensity and low fragmentation. Note that the actual peak value of the electron distribution is even lower than the applied nominal ionization energy.

Temperature profiles were measured by a K-type thermocouple for five different oven temperatures (473, 673, 873, 1073, and 1273 K) at atmospheric pressure with an argon flow of 10 slm. The jacket thermocouple was mounted in the centerline of the quartz tube at the reactor outlet and the oven, which is positioned on a slider, was then moved forward to measure the gas temperature at several oven positions to cover a relevant reactor length of 1200 mm between the thick insulation (120 mm) at the inlet of the oven furnace and the thinner insulation (40 mm) at the outlet. The measured temperature profiles have a long isothermal zone of about 800 mm inside the furnace chamber as shown in Fig 2. The quartz nozzle protrudes 20–30 mm into the reactor (see the picture in Fig. 1) so that the temperature drop at the sampling point is only about 100 K at the highest oven temperature of 1273 K and will not have an impact on the results. At lower temperatures, the temperature drop is even smaller.

Furthermore, a temperature ramp between 473 and 1273 K with 200 K/h was conducted while placing the thermocouple in the isothermal zone of the oven at 790 mm. This calibration measurement allows determination of individual centerline gas temperature profiles by using a measured temperature profile as a reference as described in [26]. Here, the temperature profile measured at an oven temperature of 1073 K was chosen as the reference to represent best the intermediate temperature range and the obtaining scaling law for a heating rate of 200 K/h and an argon gas flow of 10 slm is given in Eq. (1):

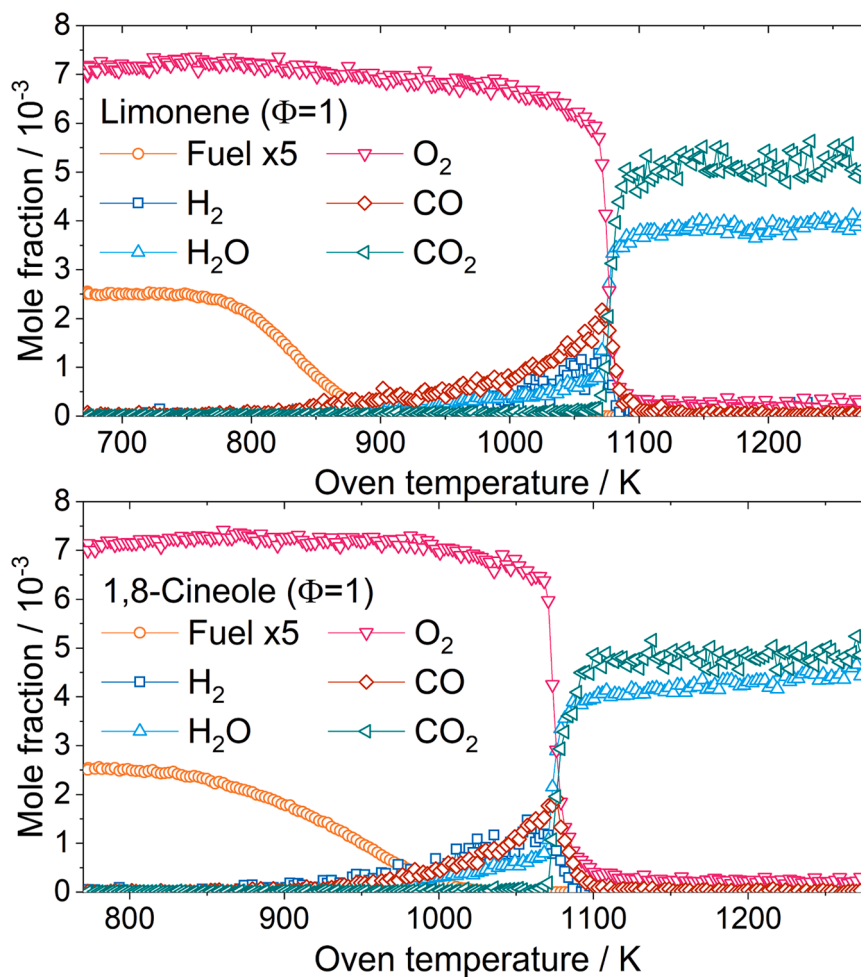


Fig. 3. Mole fraction profiles of major species (fuel, H_2 , H_2O , O_2 , CO , and CO_2) for oxidation of limonene (top) and 1,8-cineole (bottom). Note that the fuel is scaled by a factor of 5 for better visibility.

$$T(x)[K] = (T_{ref}(x) - T_0) \cdot \frac{1.0008 \cdot T_{Oven} - 14.137 \text{ K} - T_0}{T_{ref}(790 \text{ mm}) - T_0} + T_0 \quad (1)$$

In Eq. (1), $T(x)$ is the centerline gas temperature at the reactor position x for a set oven temperature T_{Oven} , $T_{ref}(x)$ is the measured centerline gas temperature at the reactor position x for an oven temperature of 1073 K, T_0 is the inlet gas temperature of 55 °C (328 K), $T_{ref}(790 \text{ mm})$ is the reference temperature measured at a reactor position of 790 mm for an oven temperature of 1073 K, and the two constants are calculated from the temperature ramp measurement with the thermocouple placed at a reactor position of 790 mm. The scaled profiles can be directly used as input for plug-flow reactor simulations and are provided in the supplementary material. These temperature profiles were scaled for oven temperatures between 370 and 1370 K with a step size of 2 K and interpolated in steps of 10 mm on the reactor axis.

3. Results and discussion

In this study, we present speciation data on oxidation and pyrolysis of limonene and 1,8-cineole measured in an atmospheric flow reactor. Quantitative mole fraction profiles are determined for individual species relative to argon according to Eq. (2):

$$x_i = \frac{S_i}{S_{Ar}} \cdot x_{Ar} \cdot \frac{1}{k_{i/Ar}(E)} \quad (2)$$

Here, x is the mole fraction and S is the integrated mass spectrometer signal, where the indices i and Ar stand for an individual species and the inert gas argon, respectively. The electron energy-dependent calibration

factor $k_{i/Ar}(E)$ is obtained from the element balance, i.e., an internal calibration strategy for major species, direct calibration measurements, or the relative ionization cross section (RICS) method. For more details about the general data reduction process and the RICS method, see references [26,28]. The absolute uncertainty of the mole fractions depends on the individual calibration method and ranges from 15 to 20 % for directly calibrated species and major species, but increases up to a factor of 2–4 when they are estimated using the RICS method [29]. Deviation of carbon balance is presented for oxidation and pyrolysis of both fuels (limonene and 1,8-cineole) in Fig. S2 in the supplementary material. It shows that the deviation is smaller than $\pm 15\%$ at all temperatures, which is in accordance with the uncertainty of directly calibrated species.

Since, to our knowledge, no kinetic model with high-temperature combustion chemistry for limonene and 1,8-cineole is currently available, the discussion on the reaction network is mainly guided by the experimental results and some previous studies from the literature, e.g., the pyrolysis of limonene [18] or the chlorine-initiated oxidation of 1,8-cineole [20,21].

3.1. Identification of impurities in limonene

For limonene, the specified purity was 97 % and potential impurities were identified by GCxGC-MS before used in the reactor experiment. As presented in Fig. S3 in the supplementary material, the GCxGC-MS analysis shows that the impurities in limonene are mainly the acyclic monoterpene β -myrcene ($C_{10}H_{16}$) and to a lesser extent some other

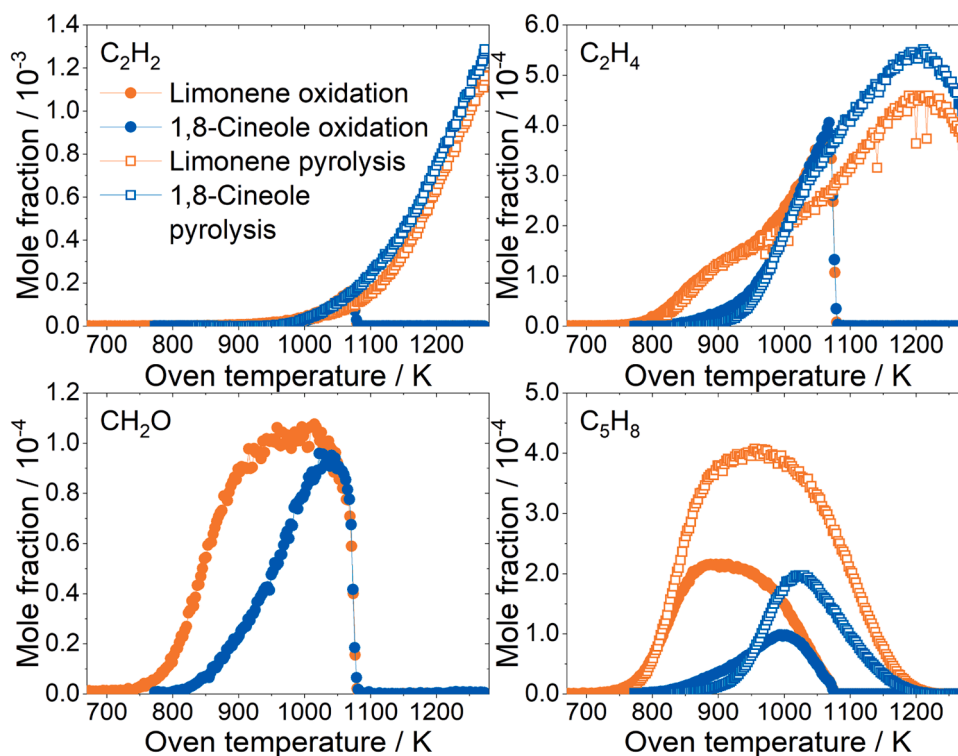


Fig. 4. Mole fraction profiles of small combustion intermediates (C_2H_2 , C_2H_4 , and CH_2O) and C_5H_8 for oxidation (closed circles) and pyrolysis (open squares) of limonene (orange symbols) and 1,8-cineole (blue symbols).

$C_{10}H_{16}$ terpenes, i.e., the monocyclic monoterpene β -phellandrene and the two bicyclic monoterpenes α -pinene and 3-carene, and the acyclic monoterpene alcohol linalool ($C_{10}H_{18}O$). Myrcene is mentioned in literature as the primary impurity present in limonene produced from orange oil [30]. Our GCxGC-MS results support this finding. Since the detected impurities are mainly limonene isomers with a share of less than 3 %, impacts on the detected species pool during limonene oxidation and pyrolysis are expected to be negligible in our flow reactor study.

3.2. Major species

For stoichiometric oxidation of limonene and 1,8-cineole, measured major species concentration profiles, i.e., reactants (fuel and O_2) and products (H_2 , H_2O , CO , and CO_2), are presented in Fig. 3 as function of the oven temperature. Limonene consumption starts at slightly lower temperatures than 1,8-cineole, i.e., 760 K compared to 820 K, and both terpene fuels are already completely consumed before significant O_2 consumption is observed, see also Fig. S4 in the supplementary material for enlarged fuel profiles of oxidation and pyrolysis. At about 1070 K, rapid consumption of the remaining O_2 is observed and CO and H_2 are completely oxidized to CO_2 and H_2O .

The different yields of H_2O reflect the different C/H and C/O ratios of the two fuel molecules, which are larger for limonene. Note that as mentioned in the experimental section, the carbon flow was constant, so that no difference in the CO_2 mole fraction is observed between the two terpene fuels. For pyrolysis, fuel consumption starts at about 30 K higher oven temperature for both terpenes as seen in Fig. S4, which also shows a comparison of the fuel mole fraction profiles during oxidation and pyrolysis.

3.3. Intermediate species

To further discuss the fuel decomposition, a deeper look into the formed intermediates during oxidation and pyrolysis of limonene and 1,8-cineole is necessary. In section 3.3.1, some typical small combustion

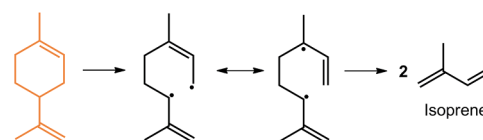
intermediates (C_1 – C_5) and aromatics are introduced first. In sections 3.3.2 and 3.3.3, some detected fuel-specific intermediates whose formation can be directly linked to first decomposition steps of the two investigated terpenes are presented and possible formation pathways are discussed individually for each fuel.

3.3.1. Small C_1 – C_5 combustion intermediates and aromatics

Fig. 4 shows the mole fraction profiles of the typical small combustion intermediates acetylene (C_2H_2), ethylene (C_2H_4), and formaldehyde (CH_2O). Additionally, the C_5H_8 mole fraction profiles are also presented in Fig. 4. C_5H_8 was calibrated as isoprene (2-methyl-1,3-butadiene) since this species is the building block of terpenes and is expected to be the main component at mass-to-charge (m/z) ratio of 68.06 as shown by photoionization mass spectrometry for combustion of other terpenes, e.g., pinenes and myrcene [31].

At stoichiometric oxidation, a steep decay in concentration is observed for the mentioned small combustion intermediates similar to the mole fraction profiles of CO and H_2 shown in Fig. 3. First appearance of C_2H_4 , CH_2O , and C_5H_8 is at significantly lower temperatures for limonene and reflects its generally higher reactivity compared to 1,8-cineole. The general shape of many intermediate mole fraction profiles is very broad for limonene, e.g., see CH_2O and C_5H_8 in Fig. 4. Maximum concentration of C_5H_8 is twice as high with limonene as the fuel and a plausible explanation might be the direct formation of isoprene over a biradical (Scheme 1) as described by Pines and Ryer [18].

For pyrolysis, ethylene (C_2H_4) decomposes at about 1200 K after passing a plateau, which is not yet reached for acetylene (C_2H_2). As



Scheme 1. Direct formation of isoprene (C_5H_8) from limonene ($C_{10}H_{16}$) over a biradical as described by Pines and Ryer [18].

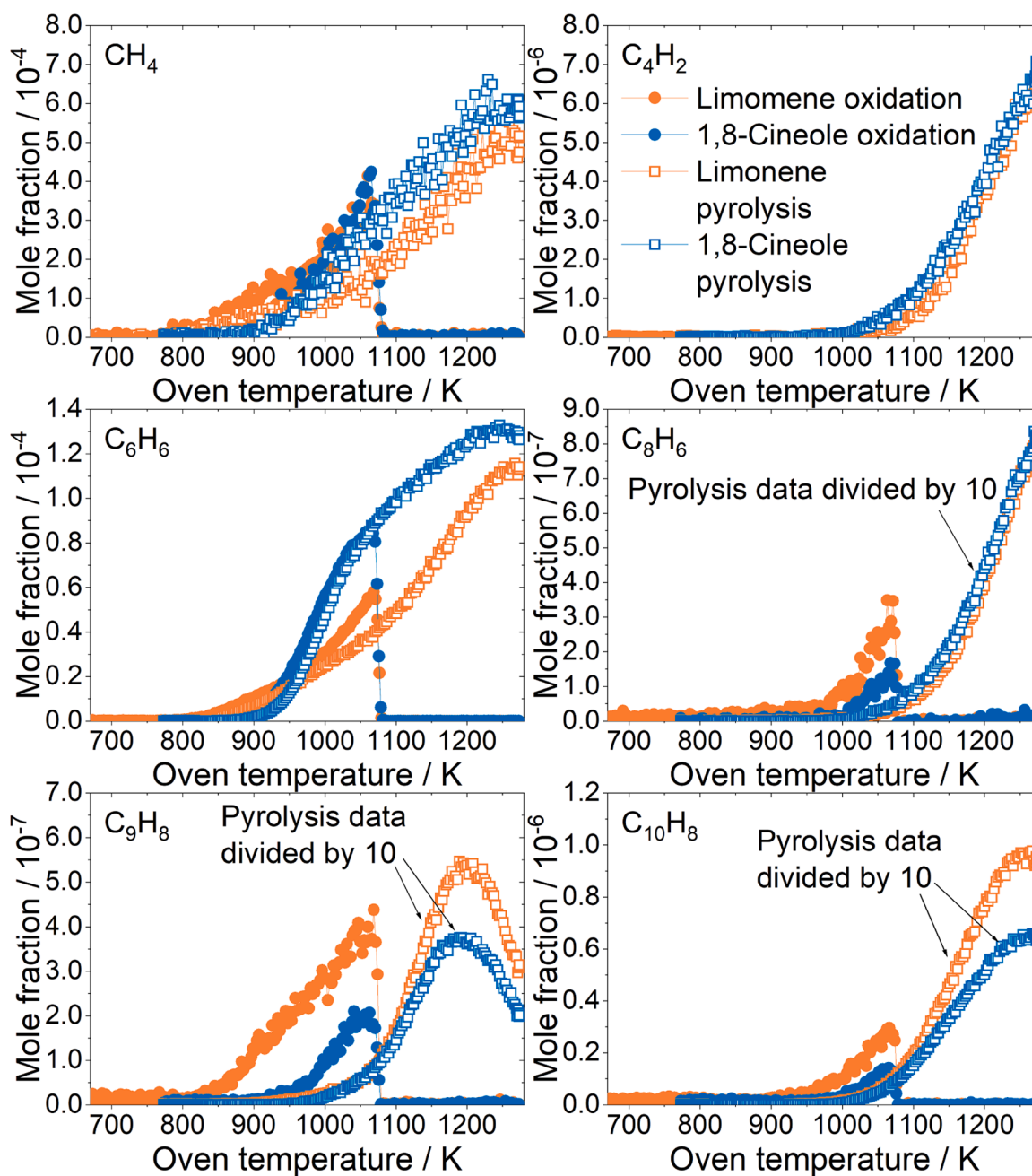


Fig. 5. Mole fraction profiles of some hydrocarbons (CH_4 , C_4H_2 , C_6H_6 , C_8H_6 , C_9H_8 , C_{10}H_8) which are present in the product gas at the highest oven temperatures during pyrolysis (open squares) of limonene (orange symbols) and 1,8-cineole (blue symbols) and comparison with oxidation data (closed circles). Mole fractions of C_8H_6 , C_9H_8 , and C_{10}H_8 from pyrolysis were divided by a factor of 10 for better visibility.

presented in Fig. 5, some other hydrocarbons, e.g., methane (CH_4), diacetylene (C_4H_2), benzene (C_6H_6), C_8H_6 , C_9H_8 , and C_{10}H_8 , also show high concentrations in the product gas at the highest reactor temperature during pyrolysis of both terpenes. Even if it is not possible to distinguish between isomers with EI-MBMS, the most likely species for C_8H_6 , C_9H_8 , and C_{10}H_8 are phenylacetylene, indene, and naphthalene based on common hydrocarbon reaction chemistry.

3.3.2. Main intermediates formed in first decomposition steps of limonene

Overall, the experimental results show that a similar species pool is formed during oxidation and pyrolysis of the two terpenes limonene and 1,8-cineole, but significant concentration differences of a factor of two or even higher are also observed for some other intermediates besides isoprene. For example, higher maximum mole fractions of C_8 – C_{10}

hydrocarbons (C_8H_{10} , C_9H_{10} , C_9H_{12} , C_9H_{14} , $\text{C}_{10}\text{H}_{12}$, and $\text{C}_{10}\text{H}_{14}$) are detected during the decomposition of limonene as seen in Fig. 6.

Most of them are probably substituted benzenes and cyclohexadienes formed from hydrogen abstraction and β -scission reactions. The lowest bond dissociation energies in limonene have the tertiary and the two secondary allylic CH bonds yielding resonance-stabilized radicals by hydrogen abstraction [32] and substituted 1,3-cyclohexadienes ($\text{C}_{10}\text{H}_{14}$) by followed β -CH-scission according to Scheme 2. *p*-Cymene ($\text{C}_{10}\text{H}_{12}$) may be then formed by another hydrogen abstraction reaction and β -scission from $\text{C}_{10}\text{H}_{14}$.

In contrast, C_9H_{14} could be formed by hydrogen addition on one of the double bonds in limonene and subsequent β -CC-scission (CH_3 elimination). Pines and Ryer explained the formation of the two monoaromatics *m*-xylene (C_8H_{10}) and *m*-ethyltoluene (C_9H_{12}) in the

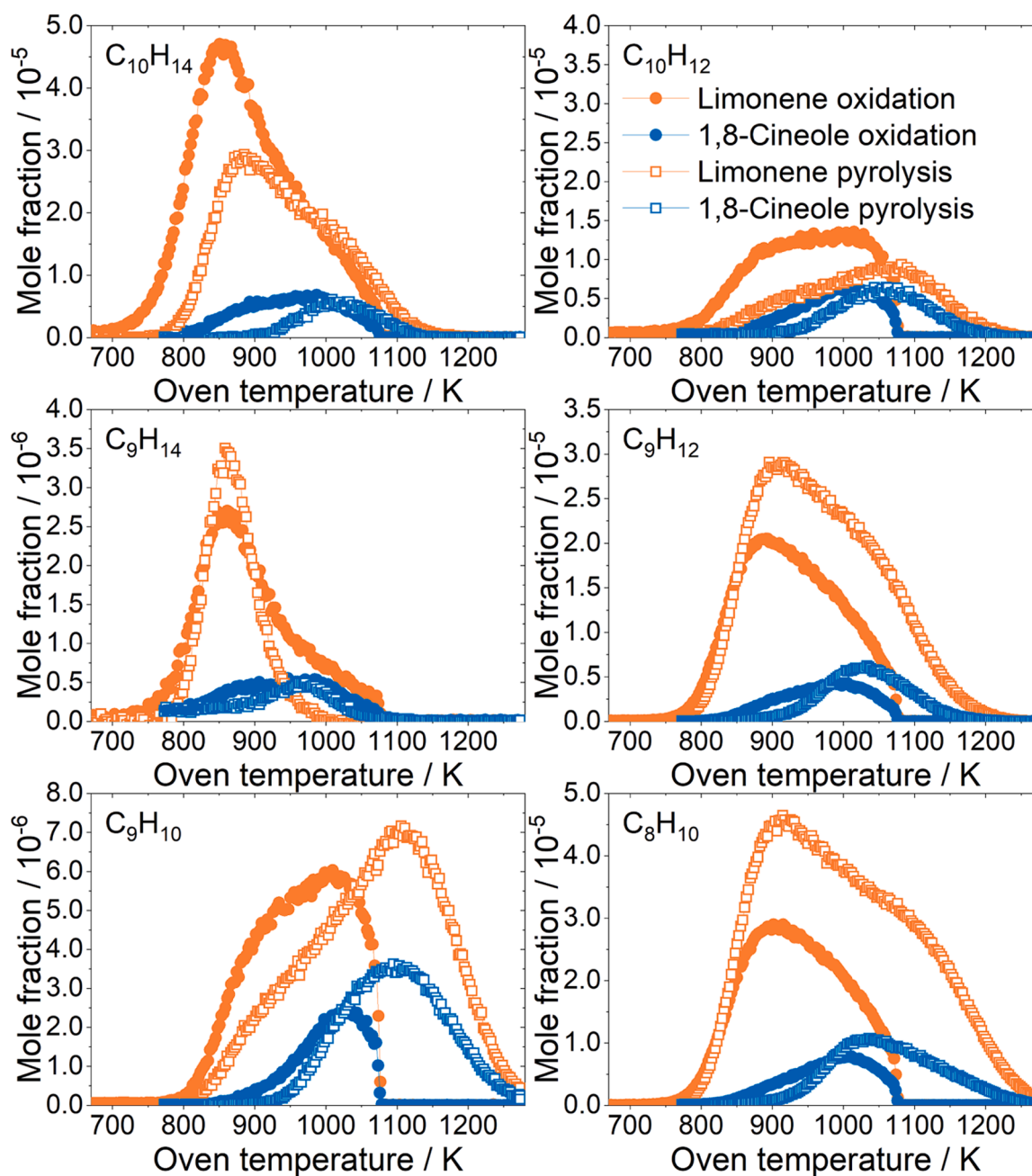


Fig. 6. Mole fraction profiles of some C_8 – C_{10} hydrocarbons formed during oxidation (closed circles) and pyrolysis (open squares) of limonene (orange symbols) and 1,8-cineole (blue symbols).

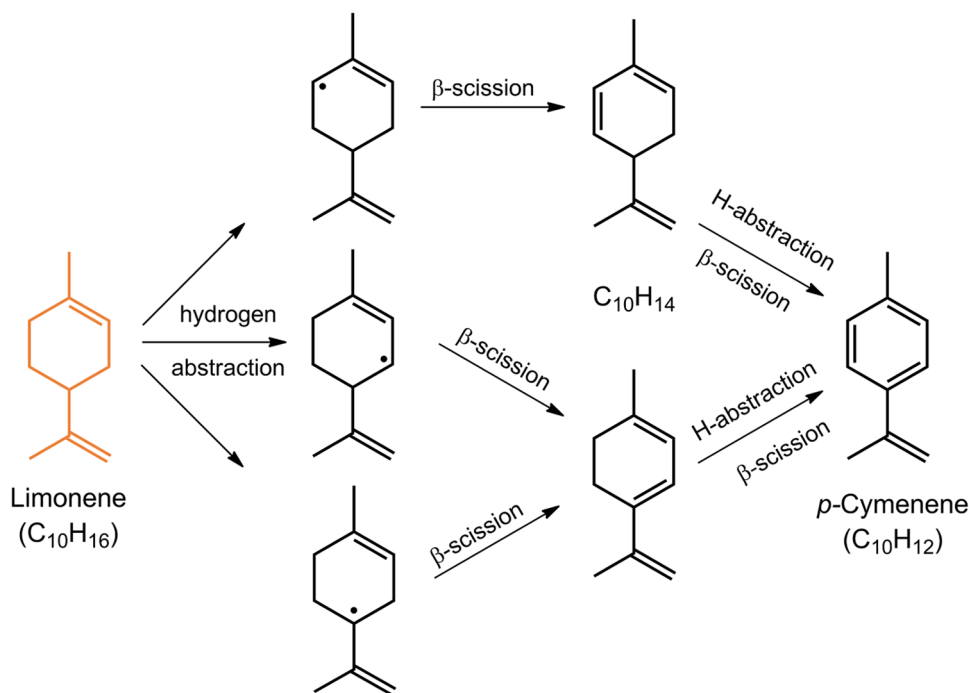
pyrolysis of limonene over a biradical and the subsequent isomerization to alkyl-substituted cyclohexadienes [18] as shown in Scheme 3.

When limonene undergoes isomerization to terpinenes ($C_{10}H_{16}$), the formation of *p*-cymene ($C_{10}H_{14}$) by hydrogen abstraction and β -CH-scission is likely (Scheme 4). Isomerization reactions of the fuel molecule were clearly observed in combustion and pyrolysis of other monoterpenes, e.g., α - and β -pinene, by photoionization mass spectrometry in flames [31] and by gas chromatography under pyrolytic conditions [33,34]. Further decomposition of *p*-cymene would then lead to toluene (C_7H_8) and propene (C_3H_6), cumene (C_9H_{12}), or 4-isopropenyltoluene ($C_{10}H_{12}$) as discussed by Obwald et al. [29] for oxidation of *p*-cymene in a similar flow reactor.

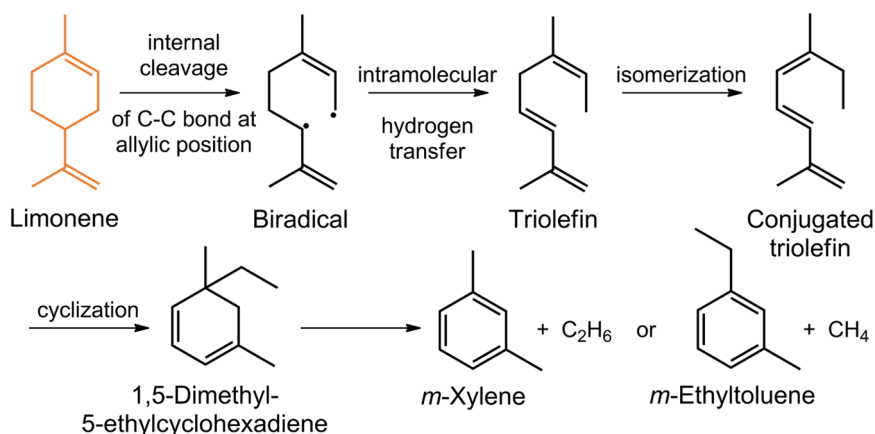
Due to the easily formation of several C_8 – C_{10} hydrocarbons during limonene oxidation and pyrolysis and the higher mole fractions of polyaromatic hydrocarbons (PAHs), e.g., indene (C_9H_8) and naphthalene

($C_{10}H_8$) (see Fig. 6), the sooting tendency seems to be generally higher for limonene and is in accordance to soot yield indices of these two terpenes from [23] and [24]. Even larger C_{11} – C_{12} hydrocarbons could be detected in the pyrolysis experiments, but were not quantified (see species profiles in the supplementary material).

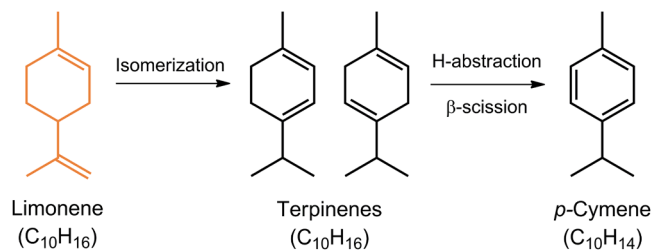
Formation of low-temperature oxidation products during oxidation of limonene in a jet-stirred reactor was observed by Dbouk et al. [13] and Benoit et al. [15] at 520–800 K and 590 K, respectively. For our investigated flow conditions, signals at m/z 150.10 ($C_{10}H_{14}O$) and 152.12 ($C_{10}H_{16}O$) were detected during oxidation of limonene with maximum peak intensity at about 824 K (see Fig. S5 in the supplementary material for mass spectra). These oxygenates with masses larger than the fuel may represent carbonyls or cyclic ethers [13] and were quantified here by calibration with 1,8-cineole as reference. They could be formed from the first oxygen addition to the fuel radical ($C_{10}H_{15}$) and



Scheme 2. Decomposition of limonene ($C_{10}H_{16}$) by hydrogen abstraction and β -scission reactions to yield substituted 1,3-cyclohexadienes ($C_{10}H_{14}$) and *p*-cymene ($C_{10}H_{12}$).



Scheme 3. Decomposition of limonene ($C_{10}H_{16}$) to yield the monoaromatics *m*-xylene (C_8H_{10}) and *m*-ethyltoluene (C_9H_{12}) according to Pines and Ryer [18].



Scheme 4. Possible isomerization of limonene ($C_{10}H_{16}$) to terpinenes ($C_{10}H_{16}$) and subsequent hydrogen abstraction and β -scission to yield *p*-cymene ($C_{10}H_{14}$).

the $C_{10}H_{17}$ radical, which itself is formed by H-addition to limonene. Subsequent isomerization to QOOH intermediates and chain propagation results then in $C_{10}H_{14}O$ and $C_{10}H_{16}O$.

3.3.3. Main intermediates formed in first decomposition steps of 1,8-cineole

C_8 – C_{10} hydrocarbons and PAHs are also formed in the oxidation and pyrolysis of 1,8-cineole, but in much lower concentrations than for limonene as presented in Figs. 5 and 6. Instead, significantly higher amounts of the hydrocarbon C_7H_{10} and the oxygenate C_3H_6O were detected with 1,8-cineole as the fuel (see Fig. 7).

During pyrolysis of 1,8-cineole, ketene (C_2H_2O), C_3H_4O , C_4H_6O , and C_4H_8O are other detected oxygenates besides C_3H_6O . Formation of C_3H_6O and C_7H_{11} could be directly linked to the fuel decomposition as described for chlorine-initiated oxidation of 1,8-cineole [20,21], i.e., starting with hydrogen abstraction reaction at one of the secondary carbon atoms adjacent to the quaternary carbon atom and followed by ring-opening and β -scission to yield acetone (C_3H_6O) and the radical C_7H_{11} (see Scheme 5).

Hydrogen abstraction at the other secondary or primary carbon atoms or at the tertiary C atom and subsequent β -CH-scission would result in larger oxygenated products at m/z 152.12 ($C_{10}H_{16}O$), which were not detected under the investigated conditions. The largest

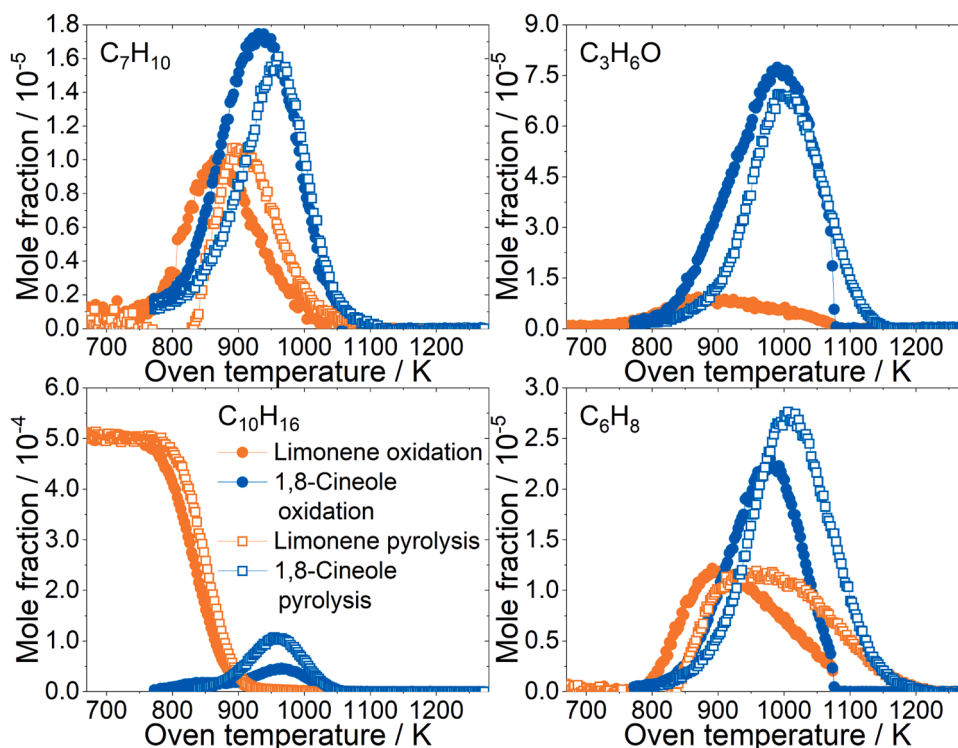
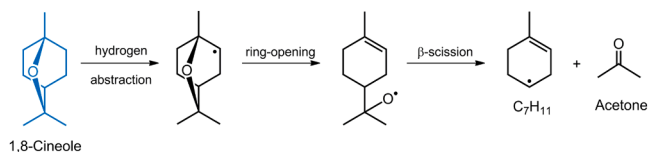


Fig. 7. Mole fraction profiles of some main intermediates formed during oxidation (closed circles) and pyrolysis (open squares) of 1,8-cineole (blue symbols) and comparison with limonene (orange symbols).

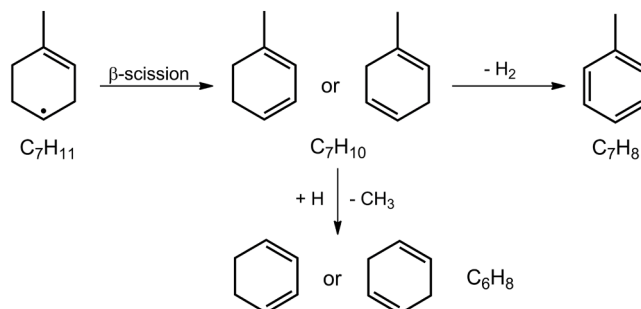


Scheme 5. Direct formation of C_7H_{11} and acetone (C_3H_6O) from 1,8-cineole ($C_{10}H_{18}O$) as described for chlorine-initiated oxidation of 1,8-cineole [20,21].

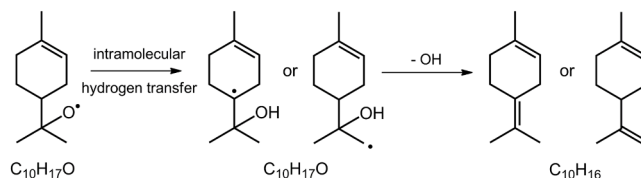
oxygenated intermediate is $C_7H_{10}O$ at m/z 110.07 and was measured in the oxidation of 1,8-cineole. In the chlorine-initiated oxidation of 1,8-cineole at 550 K, $C_7H_{10}O$ was identified as cyclic ether products formed by initial O_2 addition to C_7H_{11} followed by OH elimination [21]. Since other possible low-temperature oxidation products were not detected, $C_7H_{10}O$ may be an enol formed from C_7H_{10} by a substitution reaction with OH. C_7H_{11} radicals are a source of C_7H_{10} (1-methyl-1,3-cyclohexadiene or 1-methyl-1,4-cyclohexadiene) by β -CH-scission and further decomposition by dehydrogenation or H-addition followed by β -CC-scission leads to the formation of toluene (C_7H_8) and cyclohexadienes (C_6H_8), respectively (see Scheme 6).

As shown in Fig. 7, concentration of C_6H_8 is about a factor of two higher in the oxidation and pyrolysis of 1,8-cineole compared to the results with limonene as the fuel. According to Scheme 6, the cyclohexadienes are probably isomers of C_6H_8 in the 1,8-cineole measurements. For limonene, the presence of methylcyclopentadienes as C_6H_8 isomers is more likely and these five-membered ring species could be formed from decomposition of xylenes (C_8H_{10}). For example, *m*-xylene decomposes by H-abstraction reaction to yield xylyl radicals, which further react by ring contraction to methylcyclopentadienyl (C_6H_7) and C_2H_2 or cyclopentadiene (C_5H_6) + C_3H_3 [35,36], thus providing access to five-membered ring species.

The hydrocarbon $C_{10}H_{16}$ is also an intermediate species with 1,8-cineole as the fuel. Plausible $C_{10}H_{16}$ isomers could be terpinolene and limonene formed from the $C_{10}H_{17}O$ radical according to Scheme 7. Both $C_{10}H_{16}$ terpenes are also the main products in the catalytic dehydration



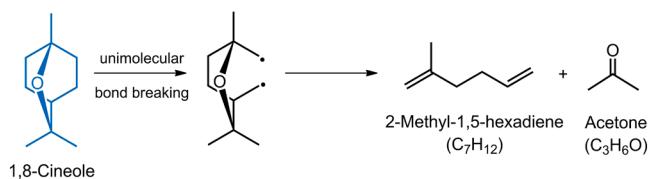
Scheme 6. Further decomposition of the C_7H_{11} radical to yield toluene and cyclohexenes (C_6H_8) over methyl-substituted cyclohexadienes (C_7H_{10}).



Scheme 7. Formation of limonene or terpinolene ($C_{10}H_{16}$) from the $C_{10}H_{17}O$ radical.

of 1,8-cineole [37]. Therefore, $C_{10}H_{16}$ was directly calibrated as limonene in our 1,8-cineole measurements.

A possible alternative formation pathway to yield directly acetone (C_3H_6O) can be described by unimolecular decomposition over a biradical according to Scheme 8. Here, 2-methyl-1,5-hexadiene (C_7H_{12}) is a byproduct. Similar decomposition steps are known for the cyclic ether tetrahydrofuran, where formaldehyde + C_3H_6 or acetaldehyde + C_2H_4 are formed by unimolecular decomposition [38]. Measured maximum mole fraction of C_7H_{12} is higher than that of C_7H_{10} showing that this route could be of relevance. Compared to the limonene measurements,



Scheme 8. Direct formation of 2-methyl-1,5-hexadiene (C₇H₁₂) and acetone (C₃H₆O) from 1,8-cineole (C₁₀H₁₈O) over a biradical.

the maximum mole fraction of C₇H₁₀ is with 1,8-cineole as the fuel a factor of 1.7 and 5 higher during oxidation and pyrolysis, respectively.

3.3.4. Comparison between oxidation and pyrolysis

For both investigated terpene fuels, the formed species pool during oxidation and pyrolysis is quite similar, but some differences can be observed. Obviously, no oxygenated species are formed during limonene (C₁₀H₁₆) pyrolysis, while even some larger oxygenated species (C₁₀H₁₄O and C₁₀H₁₆O) were detected during limonene oxidation as discussed in chapter 3.3.2. Those species may be more relevant under low-temperature conditions not studied here. Decomposition of limonene yields C₈–C₁₀ hydrocarbons in oxidation and pyrolysis (see Fig. 6). However, the route to *p*-cymene (C₁₀H₁₂) over H-abstraction reaction seems to be favored under oxidative conditions (maximum mole fractions of C₁₀H₁₄ and C₁₀H₁₂ are during oxidation a factor of 1.5 and 1.6 higher compared to pyrolysis). Since the same amount of carbon is present for oxidation and pyrolysis, direct comparison is possible. During pyrolysis, the direct formation route to aromatics (C₉H₁₂ and C₈H₁₀) according to Scheme 3 is more relevant (maximum mole fractions of C₉H₁₂ and C₈H₁₀ are during pyrolysis a factor of 1.5 and 1.6 higher compared to oxidation). This formation pathway was proposed by Pines and Ryer for limonene pyrolysis [18]. Maximum mole fraction of isoprene (C₅H₈) is under pyrolytic conditions about a factor of 2 higher compared to limonene oxidation. Therefore, direct formation of isoprene according to Scheme 1 is a more relevant route in pyrolysis.

For 1,8-cineole (C₁₀H₁₈O), some small oxygenated species besides acetone (C₃H₆O) are also formed during pyrolysis as mentioned in chapter 3.3.3. However, acetone is one of the most important species in the decomposition of 1,8-cineole. Differences in the maximum mole fraction of acetone, C₇H₁₀, and C₇H₁₂ are minor between oxidation and pyrolysis indicating that main decomposition of 1,8-cineole over Scheme 5 and 8 are most relevant under oxidative and pyrolytic conditions. More significant is the difference in the C₁₀H₁₆ concentration which is a factor of 2.3 higher under pyrolytic conditions.

4. Conclusions

Terpenes from sustainable biological sources can serve as a renewable fuel, blending component or respective precursor. A comprehensive speciation data set, measured for stoichiometric oxidation and pyrolysis of the two terpenes limonene and 1,8-cineole in a flow reactor, is presented. For the first time, detailed insights into the fuel decomposition steps in the intermediate temperature range of 673–1273 K relevant for combustion processes are gained. Generally, a similar species pool is formed, but significant concentration differences are observed for some intermediates. C₈–C₁₀ hydrocarbons are preferably formed with limonene as the fuel indicating a higher sooting tendency. In contrast, 1,8-cineole can directly yield methyl-substituted cyclohexadienes (C₇H₁₀) and acetone (C₃H₆O). Some reaction steps in the decomposition of limonene may involve initial isomerization of the fuel as known for other terpenes. To further prove these steps, flow reactor measurements with photoionization mass spectrometry, FTIR spectroscopy, or GC–MS would be useful in future to identify different isomers and to get an even deeper insight into the combustion kinetics of the two monoterpenes limonene and 1,8-cineole.

Novelty and significance statement

The novelty of this research is the detailed speciation data for stoichiometric oxidation and pyrolysis of the two terpenes limonene and 1,8-cineole, measured for the first time in a flow reactor within the intermediate temperature range of 673–1273 K relevant for combustion processes. The significance of this study lies in the insights into the initial decomposition pathways for each of the two potential biofuel candidates and the provided comprehensive data set, that can be understood as a first step towards future mechanism development and validation.

CRedit authorship contribution statement

Thomas Bierkandt: Writing – original draft, Methodology, Investigation, Formal analysis, Conceptualization. **Nina Gaiser:** Writing – review & editing, Investigation. **Jasmin Bachmann:** Writing – review & editing, Investigation. **Patrick Oßwald:** Writing – review & editing, Supervision, Funding acquisition. **Markus Köhler:** Writing – review & editing, Supervision, Funding acquisition.

Declaration of competing interest

The authors declare that they have no known competing financial interests or personal relationships that could have appeared to influence the work reported in this paper.

Acknowledgements

The authors gratefully acknowledge Jens Melder for the GCxGC-MS measurement of limonene and financial support is greatly acknowledged by the two DLR projects FFAE and NeoFuels.

Supplementary materials

Supplementary material associated with this article can be found, in the online version, at doi:10.1016/j.combustflame.2024.113854.

References

- [1] S.M.A. Rahman, T.C. Van, F.M. Hossain, M. Jafari, A. Dowell, M.A. Islam, M. N. Nabi, A.J. Marchese, J. Tryner, T. Rainey, Z.D. Ristovski, R.J. Brown, Fuel properties and emission characteristics of essential oil blends in a compression ignition engine, *Fuel* 238 (2019) 440–453.
- [2] Co-Optimization of Fuels & Engines: Fuel Properties Database, National Renewable Energy Laboratory, <https://www.nrel.gov/transportation/fuels-properties-database/>.
- [3] J.-D. Woodroffe, D.V. Lupton, M.D. Garrison, E.M. Nagel, M.J. Siirila, B.G. Harvey, Synthesis and fuel properties of high-energy density cyclopropanated monoterpenes, *Fuel Process. Technol.* 222 (2021) 106952.
- [4] X. Zhuang, O. Kilian, E. Monroe, M. Ito, M.B. Tran-Gymfi, F. Liu, R.W. Davis, M. Mirsiaghi, E. Sundstrom, T. Pray, J.M. Skerker, A. George, J.M. Gladden, Monoterpene production by the carotenogenic yeast *Rhodospiridium toruloides*, *Microb. Cell Fact.* 18 (2019) 54.
- [5] M. Musyaroh, W. Wijayanti, M.N. Sasongko, W. Winarto, The role of limonene in the branching of straight chains in low-octane hydrocarbons, *Renew. Energy* 204 (2023) 421–431.
- [6] M. Musyaroh, W. Wijayanti, M.N. Sasongko, W. Winarto, The effects of limonene and eugenol additives in n-heptane and low-octane gasoline on the emission characteristics and fuel consumption of single-cylinder gasoline engine, *Eng. Sci. Technol. Int. J.* 51 (2024) 101648.
- [7] J.-D. Woodroffe, B.G. Harvey, High-performance, biobased, jet fuel blends containing hydrogenated monoterpenes and synthetic paraffinic kerosenes, *Energy Fuels* 34 (2020) 5929–5937.
- [8] Y.-C. Hu, Y. Zhao, N. Li, J.-P. Cao, Sustainable production of high-energy-density jet fuel via cycloaddition reactions, *J. Energy Chem.* 95 (2024) 712–722.
- [9] Z. Zebec, J. Wilkes, A.J. Jervis, N.S. Scrutton, E. Takano, R. Breitling, Towards synthesis of monoterpenes and derivatives using synthetic biology, *Curr. Opin. Chem. Biol.* 34 (2016) 37–43.
- [10] B. Danon, P. van der Gryp, C.E. Schwarz, J.F. Görgens, A review of dipentene (DL-limonene) production from waste tire pyrolysis, *J. Anal. Appl. Pyrolysis* 112 (2015) 1–13.
- [11] K. Januszewicz, P. Kazimierski, W. Kosakowski, W.M. Lewandowski, Waste tyres pyrolysis for obtaining limonene, *Materials* 13 (2020) 1359.

- [12] M. Kumar, C. Tung Chong, S. Karmakar, Comparative assessment of combustion characteristics of limonene, Jet A-1 and blends in a swirl-stabilized combustor under the influence of pre-heated swirling air, *Fuel* 316 (2022) 123350.
- [13] Z. Dbouk, N. Belhadj, M. Lailliau, R. Benoit, P. Dagaut, Characterization of the autoxidation of terpenes at elevated temperature using high-resolution mass spectrometry: formation of ketohydroperoxides and highly oxidized products from limonene, *J. Phys. Chem. A* 126 (2022) 9087–9096.
- [14] Z. Dbouk, N. Belhadj, M. Lailliau, R. Benoit, P. Dagaut, On the autoxidation of terpenes: detection of oxygenated and aromatic products, *Fuel* 358 (2024) 130306.
- [15] R. Benoit, N. Belhadj, Z. Dbouk, M. Lailliau, P. Dagaut, On the formation of highly oxidized pollutants by autoxidation of terpenes under low-temperature-combustion conditions: the case of limonene and α -pinene, *Atmos. Chem. Phys.* 23 (2023) 5715–5733.
- [16] L.M. Pisarenko, D.A. Krugovov, A.N. Shchegolikhin, O.T. Kasaikina, A kinetic model for limonene oxidation, *Russ. Chem. Bull.* 57 (2008) 83–89.
- [17] L. Courty, K. Chetehouna, L. Lemée, C. Mounaïm-Rousselle, F. Halter, J.P. Garo, Pinus pinea emissions and combustion characteristics of limonene potentially involved in accelerating forest fires, *Int. J. Therm. Sci.* 57 (2012) 92–97.
- [18] H. Pines, J. Ryer, Studies in the terpene series. XXIII. Pyrolysis of *n*-limonene and of related hydrocarbons. Mechanisms of pyrolysis, *J. Am. Chem. Soc.* 77 (1955) 4370–4375.
- [19] G. Imwinkelried, E. Gaona-Colmán, M.A. Teruel, M.B. Blanco, Kinetics, mechanism and $\text{CH}_3\text{C}(\text{O})\text{CH}_3$ formation in the Cl-initiated oxidation of 1,8-cineole at 298 K and atmospheric pressure, *Chem. Phys. Lett.* 739 (2020) 136901.
- [20] J.M. Gladden, W. Wu, C.A. Taatjes, A.M. Scheer, K.M. Turner, E.T. Yu, G. O'Bryan, A.J. Powell, C.W. Gao, Tailoring next-generation biofuels and their combustion in next-generation engines, Sandia National Laboratories, 2013. Report No. SAND2013-10094.
- [21] C.W. Gao, PhD thesis, Massachusetts Institute of Technology, Cambridge, MA, USA, 2016.
- [22] S.B. Corchnoy, R. Atkinson, Kinetics of the gas-phase reactions of hydroxyl and nitrogen oxide (NO_2) radicals with 2-carene, 1,8-cineole, *p*-cymene, and terpinolene, *Environ. Sci. Technol.* 24 (1990) 1497–1502.
- [23] J. Zhu, J.V. Alegre-Requena, P. Cherry, D. Curtis, B.G. Harvey, M.A. Javed, S. Kim, C.S. McEnally, L.D. Pfeifferle, J.-D. Woodroffe, Sooting tendencies of terpenes and hydrogenated terpenes as sustainable transportation biofuels, *Proc. Combust. Inst.* 39 (2023) 877–887.
- [24] Y. Yin, P.R. Medwell, A.J. Gee, K.K. Foo, B.B. Dally, Fundamental insights into the effect of blending hydrogen flames with sooting biofuels, *Fuel* 331 (2023) 125618.
- [25] J. Melder, J. Zinsmeister, T. Grein, S. Jürgens, M. Köhler, P. Oßwald, Comprehensive two-dimensional gas chromatography: a universal method for composition-based prediction of emission characteristics of complex fuels, *Energy Fuels* 37 (2023) 4580–4595.
- [26] P. Oßwald, M. Köhler, An atmospheric pressure high-temperature laminar flow reactor for investigation of combustion and related gas phase reaction systems, *Rev. Sci. Instrum.* 86 (2015) 105109.
- [27] C.L. Rasmussen, J. Hansen, P. Marshall, P. Glarborg, Experimental measurements and kinetic modeling of $\text{CO}/\text{H}_2/\text{O}_2/\text{NO}_x$ conversion at high pressure, *Int. J. Chem. Kinet.* 40 (2008) 454–480.
- [28] C.P. Lazzara, J.C. Biordi, J.F. Papp, Concentration profiles for radical species in a methane-oxygen-argon flame, *Combust. Flame* 21 (1973) 371–382.
- [29] P. Oßwald, R. Whitside, J. Schäffer, M. Köhler, An experimental flow reactor study of the combustion kinetics of terpenoid jet fuel compounds: farnesane, *p*-menthane and *p*-cymene, *Fuel* 187 (2017) 43–50.
- [30] A.F. Thomas, Y. Bessière, Limonene, *Nat. Prod. Rep.* 6 (1989) 291–309.
- [31] T. Bierkandt, M. Hoener, N. Gaiser, N. Hansen, M. Köhler, T. Kasper, Experimental flat flame study of monoterpenes: insights into the combustion kinetics of α -pinene, β -pinene, and myrcene, *Proc. Combust. Inst.* 38 (2021) 2431–2440.
- [32] N.E.C. de Almeida, I. de Aguiar, D.R. Cardoso, Mechanism of hop-derived terpenes oxidation in beer, *J. Braz. Chem. Soc.* 26 (2015) 2362–2368.
- [33] A. Stolle, B. Ondruschka, M. Findeisen, Mechanistic and kinetic insights into the thermally induced rearrangement of α -pinene, *J. Org. Chem.* 73 (2008) 8228–8235.
- [34] A. Stolle, W. Bonrath, B. Ondruschka, Kinetic and mechanistic aspects of myrcene production via thermal-induced β -pinene rearrangement, *J. Anal. Appl. Pyrolysis* 83 (2008) 26–36.
- [35] T. Bierkandt, P. Hemberger, P. Oßwald, M. Köhler, T. Kasper, Insights in *m*-xylene decomposition under fuel-rich conditions by imaging photoelectron photoion coincidence spectroscopy, *Proc. Combust. Inst.* 36 (2017) 1223–1232.
- [36] S. Gail, P. Dagaut, Oxidation of *m*-xylene in a JSR: experimental study and detailed chemical kinetic modeling, *Combust. Sci. Technol.* 179 (2007) 813–844.
- [37] H.A. Meylemans, R.L. Quintana, M.L. Rex, B.G. Harvey, Low-temperature, solvent-free dehydration of cineoles with heterogeneous acid catalysts for the production of high-density biofuels, *J. Chem. Technol. Biotechnol.* 89 (2014) 957–962.
- [38] M. Verdicchio, B. Sirjean, L.S. Tran, P.-A. Glaude, F. Battin-Leclerc, Unimolecular decomposition of tetrahydrofuran: carbene vs. diradical pathways, *Proc. Combust. Inst.* 35 (2015) 533–541.